JPE 17-1-29

https://doi.org/10.6113/JPE.2017.17.1.294
ISSN(Print): 1598-2092 / ISSN(Online): 2093-4718

A Communicationless PCC Voltage Compensation Using an Improved Droop Control Scheme in Islanding Microgrids

Guangqian Ding[*,**], Feng Gao[†], Ruisheng Li[***], and Bingxin Wu[***]

[*,†]Key Lab of Power System Intelligent Dispatch and Control, Shandong University, Ministry of Education, Jinan, China
[**]School of Electrical Engineering, University of Jinan, Jinan, China
[***]XJ Group Corporation, Xuchang, China

Abstract

This paper proposes a point of common coupling (PCC) voltage compensation method for islanding microgrids using an improved power sharing control scheme among distributed generators (DGs) without communication. The PCC voltage compensation algorithm is implemented in the droop control scheme to reduce the PCC voltage deviation produced by the droop controller itself and the voltage drop on the line impedance. The control scheme of each individual DG unit is designed to use only locally measured feedback variables and an obtained line impedance to calculate the PCC voltage. Therefore, traditional voltage measurement devices installed at the PCC as well as communication between the PCC and the DGs are not required. The proposed control scheme can maintain the PCC voltage amplitude within an allowed range even to some extent assuming inaccurate line impedance parameters. In addition, it can achieve proper power sharing in islanding microgrids. Experimental results obtained under accurate and inaccurate line impedances are presented to show the performance of the proposed control scheme in islanding microgrids.

Key words: Droop control, Islanding microgrid, PCC voltage compensation, Power sharing

I. INTRODUCTION

Nowadays, traditional power systems are rapidly changing, and a large number of distributed generation (DG) units have being integrated into distribution power grids to form microgrids [1]-[4], which can be operated in grid-tied or islanding modes. Compared to a single DG unit, a microgrid is more appropriate to satisfy system reliability and power quality requirements. When a microgrid operates in the islanding mode, the DG units must properly share the power demand for all of the loads to ensure operational stability [5]-[11]. A key technique is to use the frequency-real power and voltage-reactive power droop control method, which has been widely used in large-scale power systems [12], [13].

Manuscript received Jun. 21, 2016 ; accepted Nov. 4, 2016
Recommended for publication by Associate Editor Il-Yop Chung.
[†]Corresponding Author: fgao@sdu.edu.cn
Tel: +86-531-81696302,Shandong University
[*]Key Lab of Power System Intelligent Dispatch and Control, Shandong University, Ministry of Education, China
[**]School of Electrical Engineering, University of Jinan, China
[***]XJ Group Corporation, China

The traditional droop control scheme can properly share the power demands by treating the grid impedance as highly inductive. However, this case is not always valid since the line impedance in low voltage microgrids is not highly inductive [14]-[16]. Therefore, the traditional droop control scheme faces the challenges of the coupling between the real and reactive power control and they cannot achieve effective power sharing [6]-[10], [14]-[17]. To solve this issue, a virtual impedance can be inserted into the control loop to regulate the equivalent impedance to be inductive or resistive [6]-[9], [14]-[17]. It has been demonstrated that the flexible operation of virtual impedance can effectively decouple the power control and improve the reactive power sharing accuracy [14], [15], [17]. However, the introduction of a virtual impedance increases the voltage drop on virtual and real line impedances. Therefore, at times the PCC voltage will be smaller than its minimum allowable value, especially under low voltage weak microgrids. This deteriorates the power quality and affects the normal load operation. Meanwhile, the performance of a power sharing scheme with a virtual impedance added depends on the

accuracy of the line impedance parameters. However, the parameters cannot be 100% accurate because the grid operation modes, temperature and other factors change the parameters of the line impedance [17]-[19]. To address these issues, a robust droop control using additional PCC voltage measurements was proposed in [20], which can achieve accurate proportional load sharing and maintain the PCC voltage quality. However, all of the inverters in [20] need an additional PCC voltage measurement unit. A hierarchical control scheme in [21] was an important step towards the standardization of microgrids, where the PCC voltage was measured and sent to all of the DG units through communication. Secondary frequency and voltage control via distributed averaging was proposed in [22], which uses localized information and nearest-neighbor communication to perform secondary control actions. An improved droop control strategy based on secondary voltage control was proposed in [23], where information on the voltage compensation signal is broadcasted from a central controller to each of the DG units. It has been demonstrated that the hierarchical control scheme can effectively restore the PCC voltage deviation. However, accurate PCC voltage control relies heavily on effective communication [24], which increases the system cost and reduce the operational reliability.

In this paper, a novel PCC voltage compensation method is implemented in a power sharing control scheme without using communication. The PCC voltage is indirectly derived from the locally measured feedback variables of the DGs and the corresponding line impedances. The proposed method can locally compensate the PCC voltage deviation produced by the droop controller itself and the voltage drop on the line impedance even assuming inaccurate line impedance parameters in the control loop. Experimental results have verified the performance of the proposed control scheme in an islanding microgrid with the accurate and inaccurate line impedance parameters obtained in the control loop.

II. Analysis of PCC Voltage Deviation

A. PCC Voltage Deviation under the Traditional Droop Control Scheme

Fig. 1 depicts a microgrid with several DGs connected in parallel and some loads connected to an ac bus, where the DG units are equipped with an energy source/energy storage system and an interfacing inverter. In addition, a static transfer switch (STS) is installed at the PCC, which is used to disconnect the microgrid from the utility grid when needed.

Generally, when a microgrid operates in the islanding mode, the well-known droop control theory takes over to achieve proper power sharing among the DGs, which regulates the frequency and amplitude of the inverter output voltage according to (1) and (2) [20]-[26]:

$$\omega_{DG} = \omega_0 - m(P_{DG} - P_0) \quad (1)$$

$$V_{DG} = V_0 - n(Q_{DG} - Q_0) \quad (2)$$

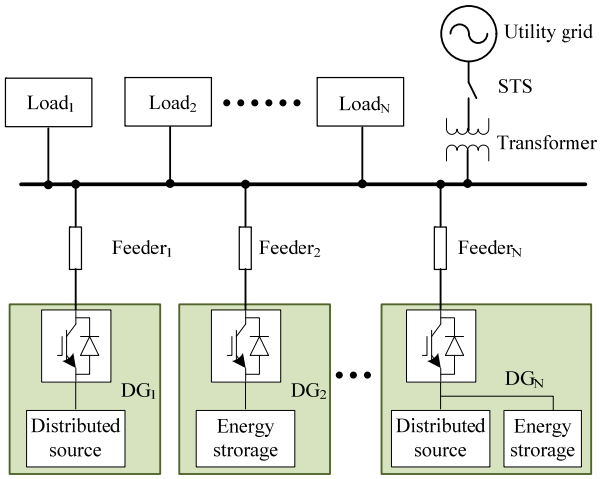

Fig. 1. General illustration of the Microgrid with DG units.

Where, ω_{DG} and V_{DG} are the DG output frequency and voltage amplitude, ω_0 and V_0 are the DG output frequency and voltage amplitude under the no load condition, m and n are the coefficients of the ω-P and V-Q droop controller, P_{DG} and Q_{DG} are the instantaneous real and reactive output power, and P_0 and Q_0 are the real and reactive power references, respectively. P_0 and Q_0 are usually set to zero when a microgrid operates in the islanding mode.

The voltage frequency and amplitude generated by (1) and (2) are used to yield the DG output voltage reference as:

$$v_{droop} = V_{DG}\sin(\int \omega_{DG} dt) \quad (3)$$

The traditional DG droop controller is illustrated in Fig. 2, where the PCC voltage can be derived as:

$$V_{PCC}(s) = V_{droop}(s) - V_{drop\_F}(s) = V_{DG}(s) - Z_F(s)I_o(s) \quad (4)$$

Where, $V_{droop}(s)$ and $V_{drop\_F}(s)$ are the output voltage of the DG unit and the voltage dropped on the feeder impedance, $Z_F(s)$ is the feeder impedance, and $I_o(s)$ is the output current of the DG unit, respectively. Due to the droop principle and the voltage drop on the feeder impedance, the PCC voltage may be smaller than its minimum allowable value when the output power of the DGs increases.

B. PCC Voltage Deviation under a Droop Control Scheme with a Virtual Impedance

When the traditional droop control scheme is implemented in a low voltage microgrid, considering the non-inductive feeder impedance, it faces the challenges of the coupling between the real and reactive power and the reactive power sharing inaccuracy. In order to properly decouple the real and reactive power control and to improve the power sharing accuracy, the output impedances of the DGs can be properly adjusted by introducing the predominant virtual inductance, which should be virtually inserted into the control loop as shown in Fig. 2, where the reference voltage v_{ref} for controlling the DG unit should be derived by considering the voltage drop on the virtual impedance [17]:

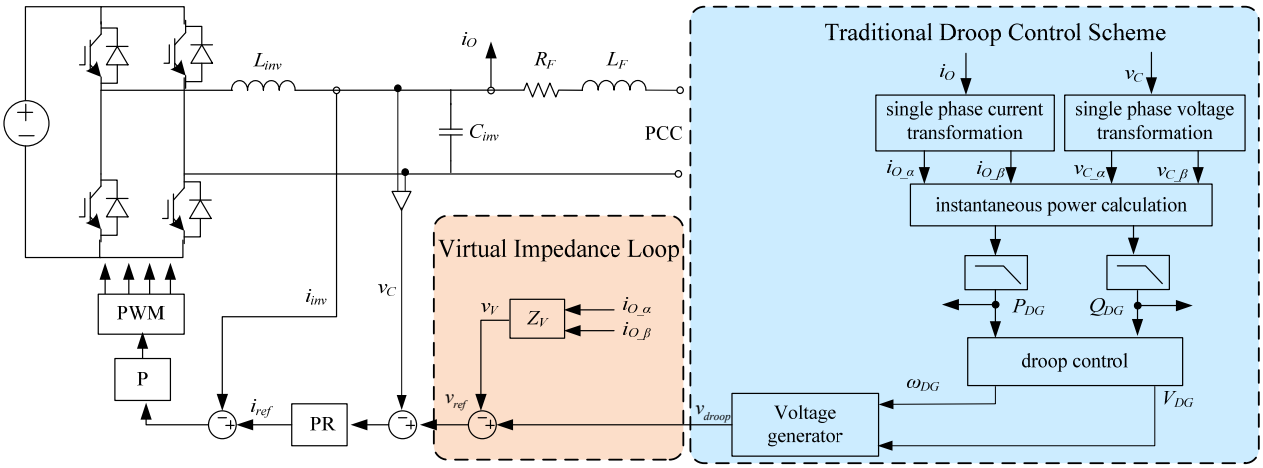

Fig. 2. Block diagram of the traditional power sharing control.

$$V_{ref}(s) = V_{droop}(s) - V_{drop\_V}(s) = V_{droop}(s) - Z_V(s)I_o(s) \quad (5)$$

Where $V_{drop\_V}(s)$ is the voltage dropped on the virtual impedance, $Z_V(s)$ is the virtual impedance, and $I_o(s)$ is the output current of the DG unit.

Usually, the virtual impedance can be selected arbitrarily to ensure that the equivalent impedance is highly inductive. Therefore, the equivalent impedance Z_E between the voltage source and the PCC can be expressed as [14]:

$$\begin{aligned} Z_E &= Z_V + Z_F = (R_V + jX_V) + (R_F + jX_F) \\ &= (R_V + R_F) + j(X_V + X_F) = R_E + jX_E \end{aligned} \quad (6)$$

Where, Z_V and Z_F are the virtual and physical feeder impedances, R_V and X_V are the virtual resistance and reactance, R_F and X_F are the physical feeder resistance and reactance, and R_E and X_E are the equivalent resistance and reactance, respectively.

Considering the voltage drop on the virtual and physical feeder impedances, the PCC voltage calculation should be updated by the following expression:

$$\begin{aligned} V_{PCC}(s) &= V_{ref}(s) - V_{drop\_F}(s) \\ &= V_{droop}(s) - Z_V(s)I_O(s) - Z_F(s)I_O(s) \\ &= V_{droop}(s) - Z_E(s)I_O(s) \end{aligned} \quad (7)$$

Compared to (4), the PCC voltage deviation may be aggravated since the total voltage drop further includes the voltage imposed on the virtual impedance.

In order to keep the microgrid stable, the voltage amplitude derived in the *V-Q* droop controller should be limited to a strict range, such as 95% of the rated voltage amplitude [9], [17]. However, when considering the voltage deviations introduced by both the *V-Q* droop controller and the voltage drop on the equivalent impedance, the PCC voltage may be smaller than the minimum allowable value as illustrated in Fig. 3, where the blue line represents the PCC voltage profile under the traditional power sharing scheme, V_0 and $V_{\min}$ are the nominal and minimum allowable values of the PCC voltage amplitude, and Q_0 is the maximum reactive power

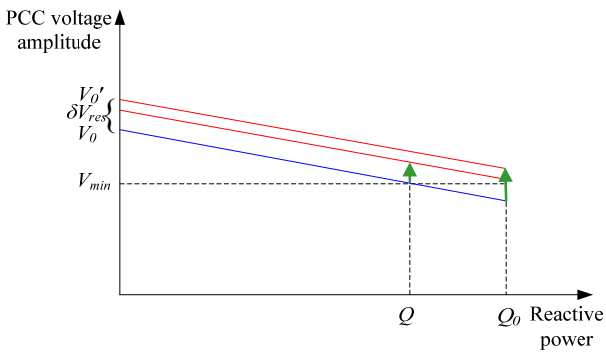

Fig. 3. PCC voltage illustration of the traditional and the proposed V-Q control principles.

injected into the microgrid. Therefore, the droop controller should be improved to consider the PCC voltage deviation by using a second-level control scheme with communication [20]-[23] or the proposed communicationless method as elaborated in the next Section.

III. Proposed Communicationless PCC Voltage Compensation Control Scheme

A. Communicationless PCC Voltage Compensation Controller

In the proposed control scheme, a PCC voltage compensation control block is embedded into the control loop to reduce the PCC voltage deviation as shown in Fig. 4. It can be seen that the variables used in the proposed scheme are only the feedback variables of the inverter itself, e.g. the output current and voltage, which can be obtained locally. Meanwhile, this does not change the coefficient n in (2), which is important for the response speed and the reactive power sharing accuracy.

This paper assumes a single-phase system to elaborate on the operational principle of the proposed method. For a three-phase system, a similar method can be employed. The

inverter output voltage and current measured locally are transformed to the α–β frame by delaying the voltage and current of a quarter-fundamental cycle for a single-phase DG unit. Its output power is calculated in the stationary artificial $\alpha-\beta$ frame as:

$$P_{DG} = \frac{\omega_{LPF}}{2(s+\omega_{LPF})}(v_{C\_\alpha} i_{O\_\alpha} + v_{C\_\beta} i_{O\_\beta}) \quad (8)$$

$$Q_{DG} = \frac{\omega_{LPF}}{2(s+\omega_{LPF})}(v_{C\_\beta} i_{O\_\alpha} - v_{C\_\alpha} i_{O\_\beta}) \quad (9)$$

Where, v_{C_α} and v_{C_β} are the DG output voltage and its quarter-cycle delayed conjugate signal, i_{O_α} and i_{O_β} are the DG output current and its quarter-cycle delayed conjugate signal, and ω_{LPF} is the cutoff frequency of the low pass filters (LPFs), respectively.

In the proposed control scheme, the real power and reactive power generated by (8) and (9) are used in the traditional droop control block to generate the voltage magnitude and phase angle. They are also adopted to calculate the voltage drop on the equivalent impedance. Taking the revised voltage vector $\vec{V}_{rev}$ as a reference vector, as shown in Fig. 5, the aforementioned P_{DG} and Q_{DG} can be used to calculate the voltage drop on the equivalent impedance as:

$$\begin{aligned}\vec{V}_{drop\_E} &= 2\left(\frac{P_{DG}R_E + Q_{DG}X_E}{V_{rev}} + j\frac{P_{DG}X_E - Q_{DG}R_E}{V_{rev}}\right) \\ &= \Delta V_{drop\_E} + j\delta V_{drop\_E}\end{aligned} \quad (10)$$

Where, $\vec{V}_{drop\_E}$ is the vector of the voltage dropped on the equivalent impedance, ΔV_{drop_E} and δV_{drop_E} are the real and imaginary components, and V_{rev} is the revised voltage amplitude of the DG, respectively.

According to Fig. 5, the relationships between the revised voltage and the PCC voltage can be derived as:

$$\vec{V}_{PCC} = \vec{V}_{rev} - \vec{V}_{drop\_E} = V_{rev} - (\Delta V_{drop\_E} + j\delta V_{drop\_E}) \quad (11)$$

In addition, the PCC voltage amplitude can be further written as:

$$V_{PCC} = \sqrt{(V_{rev} - \Delta V_{drop\_E})^2 + (\delta V_{drop\_E})^2} \quad (12)$$

In order to reduce the PCC voltage deviation, a proportional controller is used to generate the PCC voltage compensation component δV_{rev} as shown in Fig. 4.

$$\delta V_{rev} = G(s)(V_0 - V_{PCC}) = K_p(V_0 - V_{PCC}) \quad (13)$$

Where, $G(s)$ represents the transfer function of the proportional controller, V_0 and V_{PCC} are the rated and calculated amplitude of the PCC voltage, and K_p is the proportional compensation coefficient, respectively. With the PCC voltage compensation block, the voltage amplitude sent to the voltage generator needs to be updated by considering the voltage compensation component as:

$$V_{rev} = V_{DG} + \delta V_{rev} \quad (14)$$

The performance of the proposed control scheme can be demonstrated by Fig. 3, where the PCC voltage compensation controller dynamically regulates the compensated voltage δV_{rev} along with the change of the load demand to reduce the voltage deviation. It is noted that the proposed control scheme dynamically compensates the voltage deviation and that it adjusts the voltage reference vertically as the red lines shown in Fig. 3. Meanwhile, it does not change the *V-Q* droop gradient as the red lines shown in Fig. 3. Therefore, the proposed control scheme is able to maintain a response that is as fast as that of the traditional droop control scheme.

B. Performance Analysis of the Proposed PCC Voltage Compensation Method

Considering that the real component ($V_{rev} - \Delta V_{drop\_E}$) is much greater than the imaginary component (δV_{drop_E}) expressed in (12), the PCC voltage amplitude in (12) can be approximately rewritten as:

$$\begin{aligned}V_{PCC} &\approx \sqrt{(V_{rev} - \Delta V_{drop\_E})^2} \\ &= V_{rev} - \Delta V_{drop\_E} \\ &= V_{rev} - \frac{2(P_{DG}R_E + Q_{DG}X_E)}{V_{rev}}\end{aligned} \quad (15)$$

When the power generation of the DG reaches its power rating under the traditional droop control scheme with the virtual impedance, the voltage amplitude generated from the droop controller is reduced to its minimum allowable value (e.g. 95% of the rated voltage), and the PCC voltage amplitude can be derived as:

$$V_{PCC} = V_{\min} - \frac{2(P_0R_E + Q_0X_E)}{V_{\min}} \quad (16)$$

From (16), the largest deviation below the allowable minimum value of the PCC voltage (e.g. 95% of the rated voltage) can be expressed as:

$$\Delta V_{PCC} = \frac{2(P_0R_E + Q_0X_E)}{V_{\min}} \quad (17)$$

In order to keep the PCC voltage within the designed allowable range, the PCC voltage compensation control scheme should have the capability to eliminate the largest deviation in (17). When the power generation of the DG reaches its power rating under the proposed control scheme, the PCC voltage should be larger than the allowable minimum value expressed as:

$$\begin{aligned}V_{PCC} &= V_{rev} - \frac{2(P_0R_E + Q_0X_E)}{V_{rev}} \\ &= V_{\min} + K_p(V_0 - V_{\min}) - \frac{2(P_0R_E + Q_0X_E)}{V_{\min} + K_p(V_0 - V_{\min})} \geq V_{\min}\end{aligned} \quad (18)$$

From (18), the proportional compensation coefficient can be derived as the following expression:

$$K_p \geq \frac{\sqrt{V_{\min}{}^2 + 8(P_0R_E + Q_0X_E)} - V_{\min}}{2(V_0 - V_{\min})} \quad (19)$$

On the other hand, the DG voltage should not exceed its

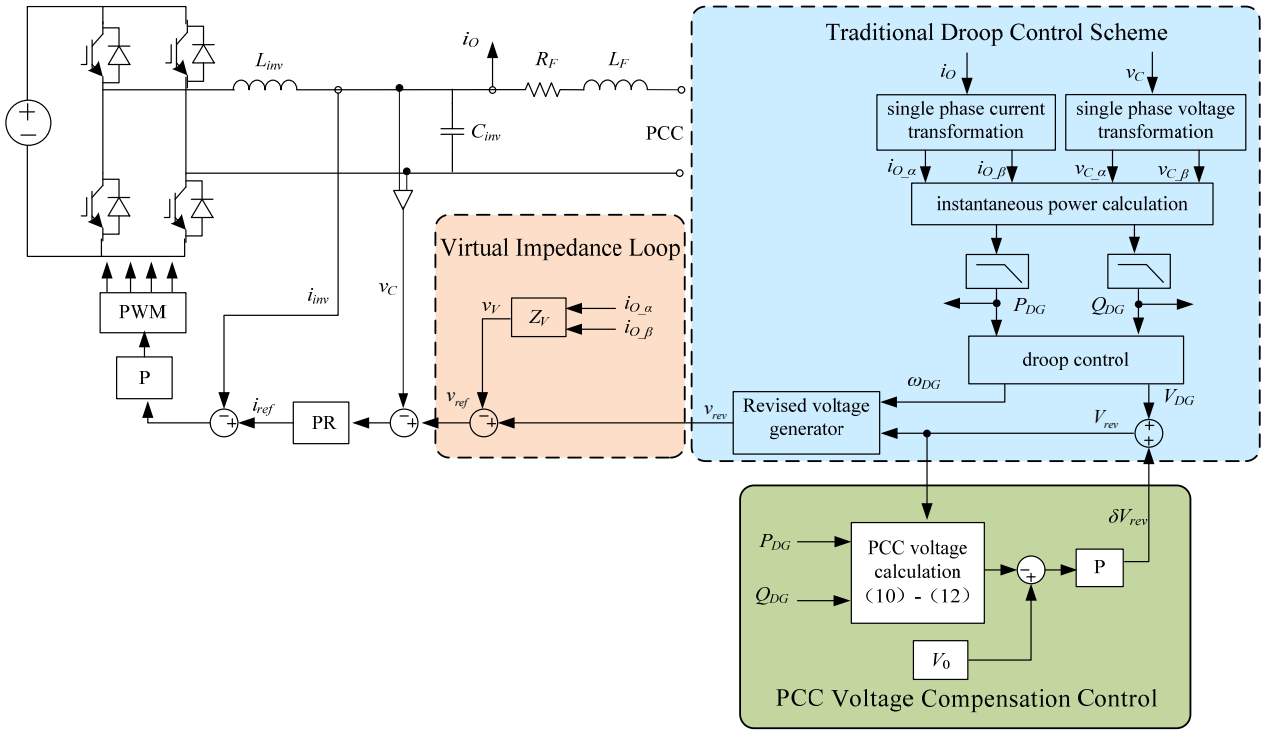

Fig. 4. Block diagram of the proposed power sharing control.

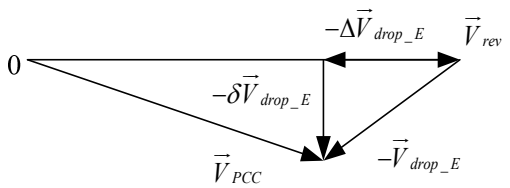

Fig. 5. Vector diagram of the PCC voltage calculation.

maximum allowable value. Therefore, the revised voltage of the DG unit should be smaller than the allowable maximum value expressed as:

$$V_{rev} = V_{DG} + \delta V_{rev} = V_{\min} + K_p(V_0 - V_{\min}) \le V_{\max} \quad (20)$$

From (20), the proportional compensation coefficient can be derived as the following expression:

$$K_p \le \frac{V_{\max} - V_{\min}}{V_0 - V_{\min}} \quad (21)$$

From (18) to (21), it can be seen that the rated power, the rated voltage and the designed range of the voltage are known values for a microgrid. The virtual impedance and the equivalent impedance design have been analyzed in [14]. Therefore, their descriptions are not shown here for the sake of brevity. The range of compensation coefficient K_p can be determined for maintaining the PCC voltage within the designed range.

In practice, the line impedance parameters obtained for the PCC voltage compensation calculation deviate from the real value mainly due to changes in the grid operation modes and temperature. Therefore, it is necessary to analyze the performance of the proposed PCC voltage compensation method under inaccurate line impedance calculation conditions. It is assumed that the actual feeder impedance is γ times the feeder impedance obtained for the calculation. In this case, the PCC voltage in (18) can be rewritten as:

$$V_{PCC} = V_{rev} - \frac{2P_0(\gamma R_F + R_V) + 2Q_0(\gamma X_F + X_V)}{V_{rev}}$$
$$= V_{\min} + K_p(V_0 - V_{\min}) - \frac{2\gamma(P_0R_F + Q_0X_F) + 2(P_0R_V + Q_0X_V)}{V_{\min} + K_p(V_0 - V_{\min})}$$
$$\ge V_{\min} \quad (22)$$

$$\gamma \le \frac{K_p(V_0 - V_{\min}) \cdot (V_{\min} + K_p(V_0 - V_{\min})) - 2(P_0R_V + Q_0X_V)}{2(P_0R_F + Q_0X_F)} \quad (23)$$

It is noted that the designed compensation coefficient K_p can tolerate the line impedance deviation in the PCC voltage compensation calculation as long as it can remain (23) effective under the designed operation conditions. Therefore, K_p can be designed according to (19) and (21) and further selected by considering the parameter accuracy of the line impedance. Doing so, the PCC voltage can be effectively compensated.

C. Inverter Control Strategy

The voltage frequency and the revised amplitude generated by (1) and (14) are used to yield the revised DG output voltage reference as:

$$v_{rev} = V_{rev} \sin(\int \omega_{DG} dt) \quad (24)$$

Considering the virtual impedance inserted into the control strategy, as shown in Fig. 4, the output voltage reference can

be modified as:

$$v_{ref} = v_{rev} - v_V = v_{rev} - (R_V i_{O\_\alpha} - \omega_0 L_V i_{O\_\beta}) \quad (25)$$

Where, v_V is the voltage drop on the virtual impedance, and R_V and L_V are the virtual resistance and inductance.

In order to realize proper voltage tracking performance, a double loop controller was adopted as shown in Fig. 4. The voltage control loop uses a proportional controller plus a resonant controller to achieve proper voltage tracking performance as expressed below:

$$G_{outer}(s) = K_{uP} + \frac{2K_{uR}\omega_c s}{s^2 + 2\omega_c s + \omega_0^2} \quad (26)$$

Where, K_{uP} is the proportional gain, K_{uR} is the resonant gain, ω_c is the cutoff angular frequency for the resonant bandwidth control, and ω_0 is the nominal fundamental angular frequency, respectively. It can realize almost zero steady-state error compensation by means of a proper gain selection.

In order to improve the dynamic performance, a current control loop is embedded in the outer voltage control loop. The filter inductor current is measured as feedback for the inner current control loop. A proportional controller is used to force the feedback current to track the reference as:

$$G_{inner}(s) = K_{iP} \quad (27)$$

Where, K_{iP} is the proportional gain. The current control loop is used to produce the desired modulation signals, which are sent to the pulse width modulation (PWM) generator, as shown in Fig. 4.

IV. Experimental Verification

To validate the performance of the proposed PCC voltage compensation scheme, a single-phase islanding microgrid was implemented in the laboratory as shown in Fig. 6. The microgrid consists of two H-bridge-based DG units with the same power rating and a conventional RL load connected to the PCC. The minimum voltage V_{min} is set to 95% of the rated voltage. The developed control algorithm is executed on a dSPACE1103 real-time platform. The detailed circuit and control parameters are listed in Table I.

A. Experimental Results with Accurate Feeder Impedances

Experiment 1: First, a conventional RL load of 40Ω, 20mH was connected to the PCC. Both of the DGs were under the droop control method with a virtual impedance, as presented in Fig. 2, before 0.2s. Then at 0.2s the PCC voltage compensation method, as presented in Fig. 4, was activated for both of the DGs simultaneously. The captured experimental waveforms were presented in Fig. 7. Spectrum analyses of the PCC voltages under both of the controllers are shown in Fig. 8. It can be seen that the PCC voltage changes from 151.2V to 152.2V after the PCC voltage compensation is activated. Therefore, the proposed PCC voltage compensation method can effectively reduce the PCC voltage deviation. The output currents of both of the DGs rapidly

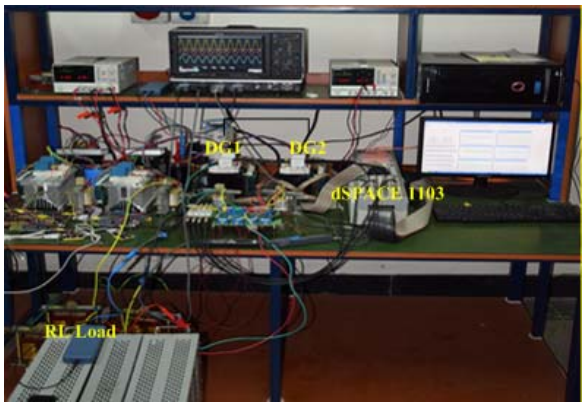

Fig. 6. Photograph of experimental prototype.

TABLE I
Parameters Used in Experiment

Parameters	Values
Nominal PCC voltage (peak value)	155.54V
Rated fundamental frequency	50Hz
DC link voltage	200V
Rated real power	500W
Rated reactive power	50var
Inverter switching frequency	12.5kHz
Inverter output filter inductance	2mH
Inverter output filter capacitance	20μF
DG1 feeder impedance	0.1Ω, 2mH
DG2 feeder impedance	0.2Ω, 3mH
DG1 virtual impedance in experiment A	0.1Ω, 1mH
DG1 virtual impedance in experiment B	0.125Ω, 1.5mH
K_p	0.3

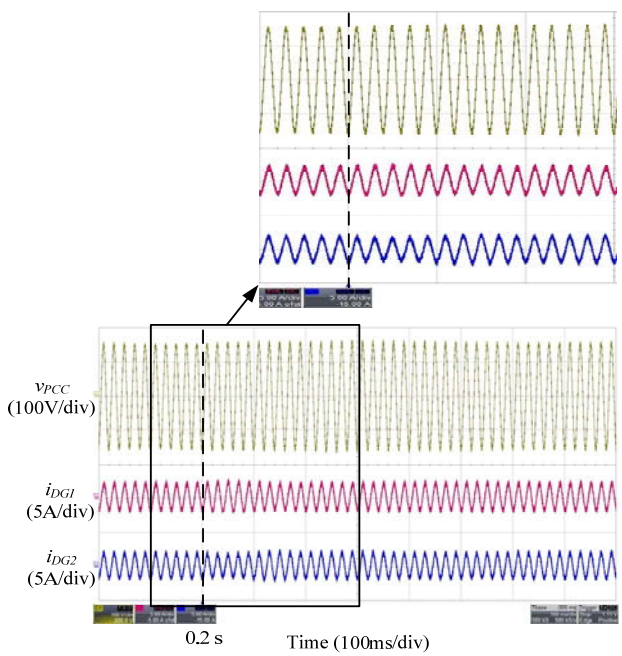

Fig. 7. Captured experimental results with accurate impedance when using the droop control method before 0.2s and the proposed method after 0.2s. (from TOP to BOTTOM: PCC voltage, line current of DG unit 1 and line current of DG unit 2).

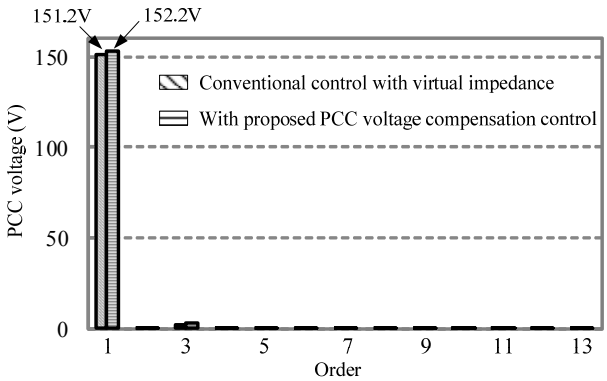

Fig. 8. Spectrum analysis of PCC voltages before and after 0.2s.

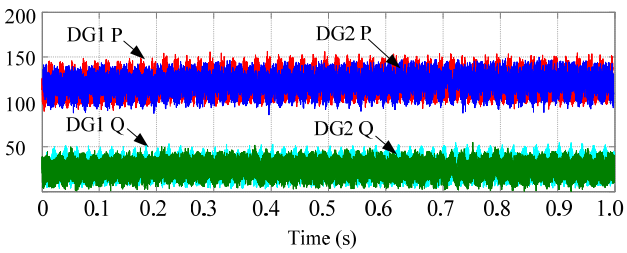

Fig. 9. Power sharing performance of both DGs.

respond to the proposed scheme as shown in Fig.7, and the THD values of i_{DG1} and i_{DG2} are 4.85% and 4.8%, respectively. The real and reactive power can be properly shared by both of the DGs as shown in Fig. 9. It is noted that a small increase in the real and reactive power after 0.2s appears due to the activated PCC voltage compensation method.

Experiment 2: First, a conventional RL load of 40Ω, 20mH was connected to the PCC. Then another conventional RL load of 40Ω, 20mH was connected to the PCC at 0.2s. Both of the DGs were conducted under the traditional droop control scheme with a virtual impedance. Fig. 10 shows experimental results before and after the load change at 0.2s. It is noted that the PCC voltage has an obvious drop after 0.2s. Fig. 11 shows detailed spectrums of the PCC voltages before and after 0.2s. It can be seen that the PCC voltage amplitude after 0.2s has been reduced to 147.1V, which is smaller than the minimum allowable value of 147.7V. The output currents for both of the DGs increase rapidly to respond to the load change, and the THD values of i_{DG1} and i_{DG2} are 2.47% and 2.44% after the load change. Although both of the DGs can still properly share the power demands, as shown in Fig. 12, the PCC voltage deviation can be further regulated to maintain the power quality.

Experiment 3: To further evaluate the performance of the proposed communication-less PCC voltage compensation method with a load change, Experiment 2 was conducted again where both of the DGs are under the proposed compensation method all the time. Fig. 13 shows experimental results where the proposed PCC voltage compensation method kept the PCC voltage amplitude within

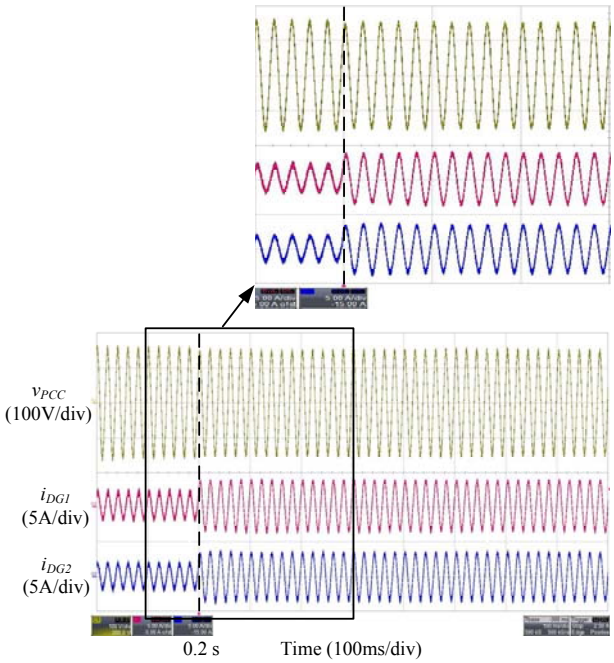

Fig. 10. Captured experimental results with accurate impedance when using the traditional droop control method with the load change at 0.2s. (from TOP to BOTTOM: PCC voltage, line current of DG unit 1 and line current of DG unit 2).

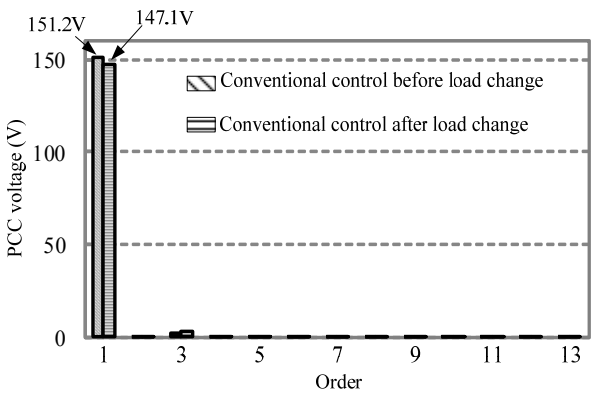

Fig. 11. Spectrum analysis of PCC voltages before and after 0.2s.

the allowable range all the time. In addition, the spectrum in Fig. 14 can demonstrate the performance more precisely, where the PCC voltage amplitude is changed from 152.2V to 148.9 after a load change. Comparing the results from experiment 2 with those from the conventional control, as shown in Fig. 11, the PCC voltage is kept within the allowable range. Meanwhile, compared with Fig. 12, it can be seen that the DGs currents response speed of the proposed method is the same as that of the traditional method. In addition, the THD values of i_{DG1} and i_{DG2} are 2.45% and 2.43%, respectively. The proposed method can achieve proper power sharing between both of the DGs as shown in Fig. 15.

B. Experimental Results with Inaccurate Feeder Impedances

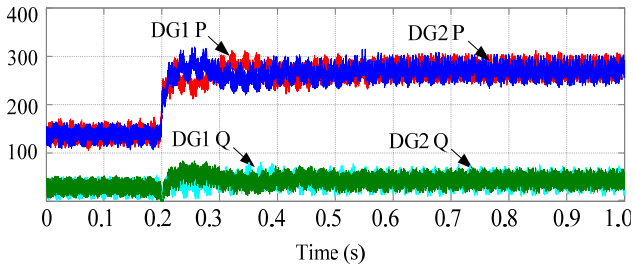

Fig. 12. Power sharing performance of both DGs under the traditional droop control method with the virtual impedance.

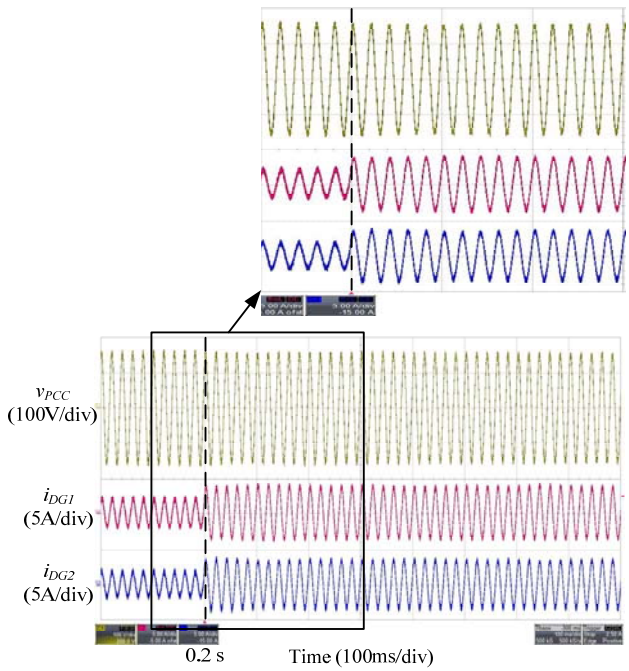

Fig. 13. Captured experimental results with accurate impedance when using the proposed method with the load change at 0.2s. (from TOP to BOTTOM: PCC voltage, line current of DG unit 1 and line current of DG unit 2).

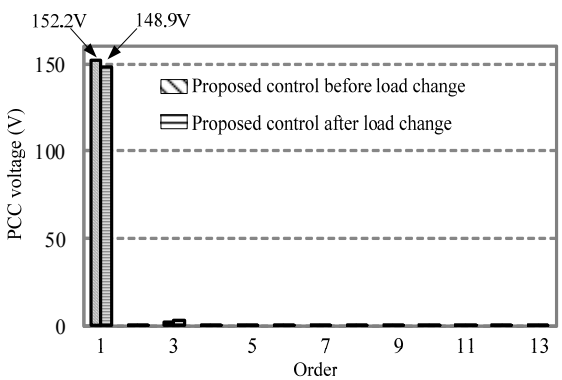

Fig. 14. Spectrum analysis of PCC voltages before and after 0.2s.

To further verify the effectiveness of the PCC voltage compensation method, similar experimental verification methods were conducted with inaccurate feeder impedances, where the measured feeder impedance of DG unit 1 is 75% of the real impedance. In this case, the measured feeder

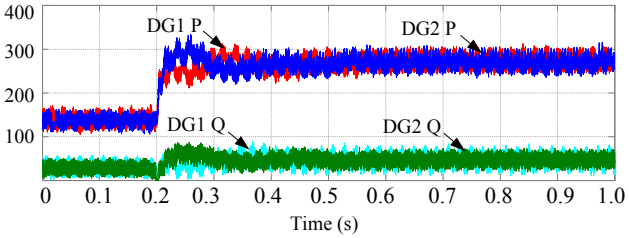

Fig. 15. Power sharing performance of both DGs under the proposed control method.

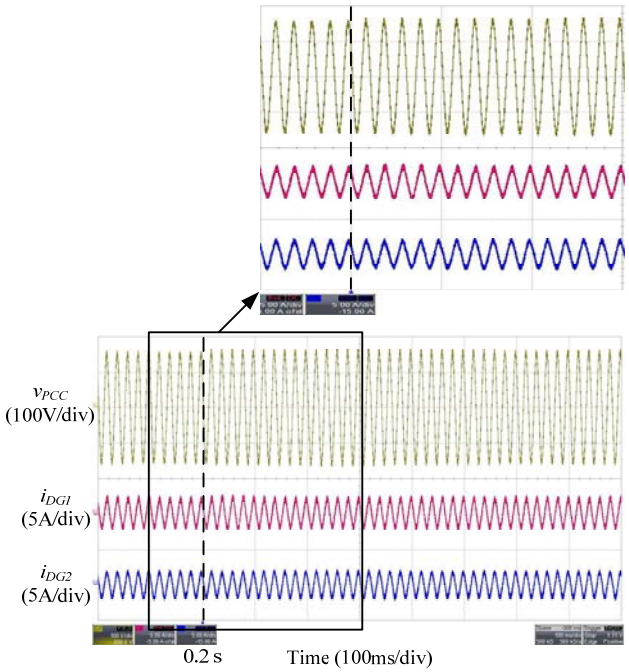

Fig. 16. Captured experimental results with inaccurate impedance when using the droop control method before 0.2s and the proposed method after 0.2s. (from TOP to BOTTOM: PCC voltage, line current of DG unit 1 and line current of DG unit 2).

resistance and inductance for the controller calculation are 0.075Ω and 1.5mH, respectively. According to (6), the virtual impedance of DG unit 1 should be set to 0.125Ω and 1.5mH for achieving the proper power sharing.

Experiment 4: An experimental verification procedure that is similar to Experiment 1 was conducted with an inaccurate feeder impedance. Fig. 16 shows the captured waveforms of the PCC voltage and DG units output currents. A spectrum analysis of the PCC voltage under both control methods is shown in Fig. 17. It can be seen that the proposed PCC voltage compensation control can effectively reduce the PCC voltage deviation when assuming an inaccurate feeder impedance, where the PCC voltage increases from 151.2V to 152.1V. The output currents for both of the DGs rapidly respond to the proposed scheme as shown in Fig. 16, and the THD of i_{DG1} and i_{DG2} are 4.87% and 4.84%, respectively. Due to the fact that the whole microgrid has the same operation frequency in the steady-state condition, the DG units can accurately share the real power demand. However, the

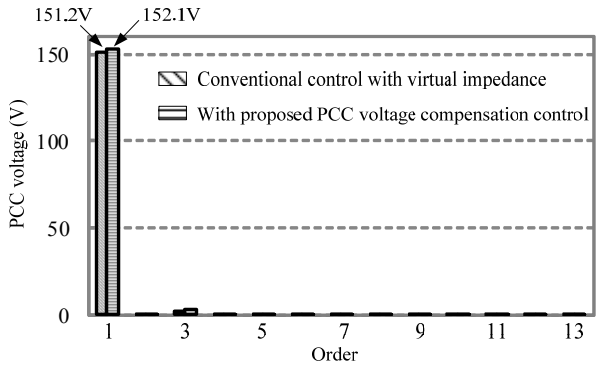

Fig. 17. Spectrum analysis of PCC voltages before and after 0.2s.

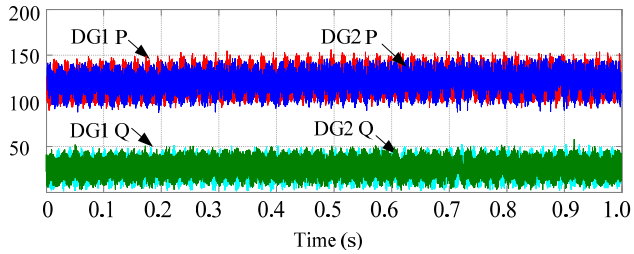

Fig. 18. Power sharing performance of both DGs.

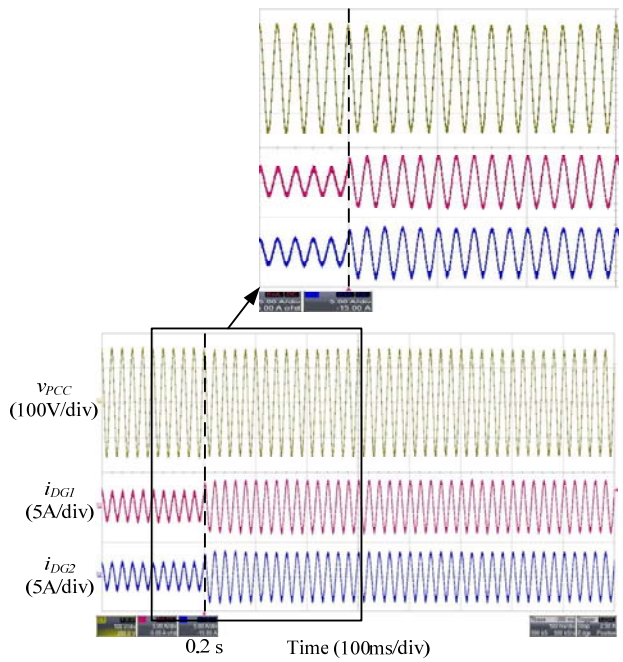

Fig. 19. Captured experimental results with inaccurate impedance when using the traditional droop control method with the load change at 0.2s. (from TOP to BOTTOM: PCC voltage, line current of DG unit 1 and line current of DG unit 2).

accuracy of the reactive power sharing is affected by the inaccurate feeder impedance as shown in Fig. 18, where the reactive power generated from both of the DGs are 23var and 23.5var before 0.2s, and 23.2var and 24var after 0.2s.

Experiment 5: An experimental verification procedure that is similar to Experiment 2 was conducted with an inaccurate feeder impedance. Fig. 19 shows experimental results under the traditional droop control scheme with an inaccurate feeder

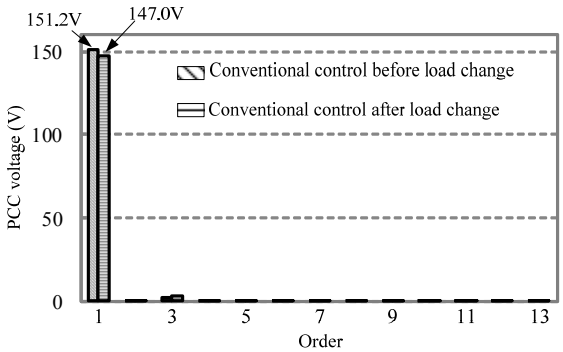

Fig. 20. Spectrum analysis of PCC voltages before and after 0.2s.

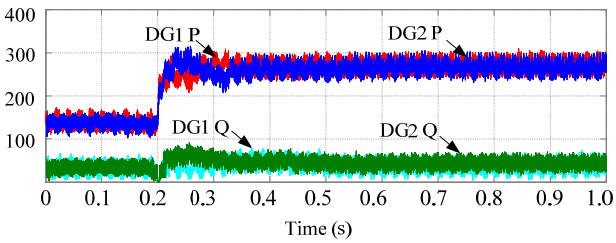

Fig. 21. Power sharing performance of both DGs under the traditional droop control method with the virtual impedance.

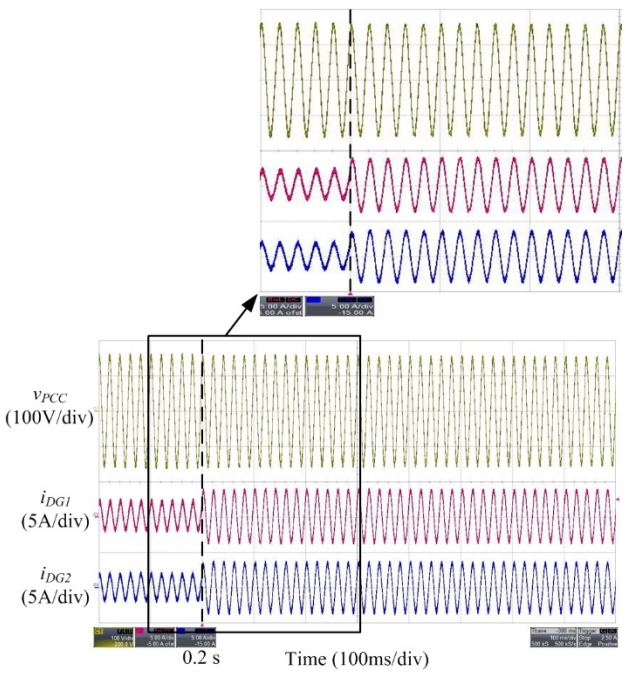

Fig. 22. Captured experimental results with inaccurate impedance when using the proposed method with the load change at 0.2s. (from TOP to BOTTOM: PCC voltage, line current of DG unit 1 and line current of DG unit 2).

impedance. Fig. 20 shows the detailed spectrums of the PCC voltages before and after 0.2s. It can be seen that the PCC voltage amplitude after 0.2s is reduced to 147.0V, which is smaller than the allowable minimum value. The output currents for both of the DGs increase rapidly to respond to the load change, and the THDs of i_{DG1} and i_{DG2} are 2.50% and

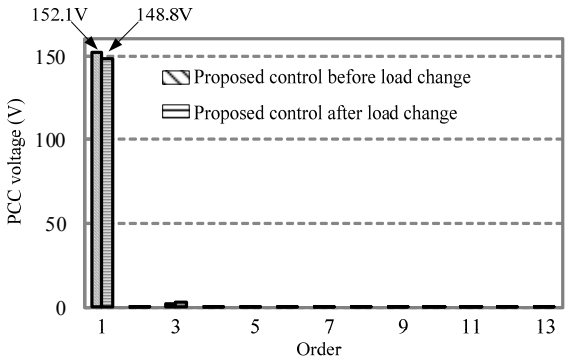

Fig. 23. Spectrum analysis of PCC voltages before and after 0.2s.

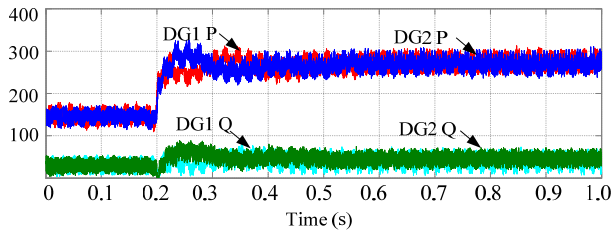

Fig. 24. Power sharing performance of both DGs under the proposed control method.

2.46%, respectively. As demonstrated in Fig. 21, the real power sharing between both of the DGs can maintain the accuracy. Meanwhile DG unit 1 shares less reactive power due to a feeder 1 impedance measurement error.

Experiment 6: An experimental verification procedure that is similar to Experiment 3 was conducted with an inaccurate feeder impedance. Fig. 22 shows experimental results using the proposed communicationless PCC voltage compensation method before and after the load change at 0.2s. From the spectrum illustrated in Fig. 23, it can be seen that the PCC voltage amplitude was changed from 152.1V to 148.8V after the load demand was increased. Comparing the results obtained in Experiment 5 with the conventional control as shown in Fig. 19 and Fig. 20, the PCC voltage deviation is significantly improved, and the PCC voltage can be maintained within the allowable range. Meanwhile, the DGs currents response speed of the proposed scheme is the same as that in Experiment 5 with the conventional control scheme, and the THD values of i_{DG1} and i_{DG2} are 2.47% and 2.44%, respectively. Both of the DG units can still properly share the real power demands, while the reactive power sharing accuracy is influenced by the feeder 1 impedance measurement error as shown in Fig. 24.

V. Conclusions

This paper proposes a novel communicationless PCC voltage compensation method for islanding microgrids by improving the power sharing control scheme among the DGs to compensate the PCC voltage deviation produced by the droop control algorithm and the voltage drop on the impedance. The control scheme for each of the individual DG units was designed to derive the PCC voltage with the locally measured feedback variables of the inverter itself and the obtained feeder impedance. Therefore, the traditional voltage measurement device installed at the PCC as well as the communications between the PCC and the DGs are not required. The proposed control scheme can maintain the PCC voltage within an allowable range even assuming inaccurate feeder impedances parameters. Experimental results verified the performance of the proposed method under accurate and inaccurate impedance measurement conditions.

References

[1] X. Wang, J. M. Guerrero, F. Blaabjerg, and Z. Chen, "A review of power electronics based microgrids," *Journal of Power Electronics*, Vol. 12, No. 1, pp. 181-192, Jan. 2012.

[2] J. M. Guerrero, P. C. Loh, L. Tzung-Lin, and M. Chandorkar, "Advanced control architectures for intelligent microgrids – Part II: Power quality, energy storage, and AC/DC microgrids," *IEEE Trans. Ind. Electron*., Vol. 60, No. 4, pp. 1398-1405, Apr. 2013.

[3] G. Q. Ding, F. Gao, R. Wei, K. Zhou, "Communication-Less harmonic compensation in a multi-bus microgrid through autonomous control of distributed generation grid-interfacing converters," *Journal of Modern Power Systems and Clean Energy*, Vol. 3, No. 4, pp. 597-609, Dec. 2015.

[4] Q. Zhang, Y. Liu, C. Wang, and N. Wang, "Parallel operation of microgrid inverters based on adaptive sliding-mode and wireless load-sharing controls," *Journal of Power Electronics*, Vol. 15, No. 3, pp. 741-752, Mar. 2015.

[5] J. W. He, Y. W. Li, J. M. Guerrero, F. Blaabjerg, and J. C. Vasquez, "An islanding microgrid power sharing approach using enhanced virtual impedance control scheme," *IEEE Trans. Power Electron.*, Vol. 28, No. 11, pp. 5272-5282, Nov. 2013.

[6] W. Issa , S. Sharkh, T. Mallick, and M. Abusara, "Improved reactive power sharing for parallel-operated inverters in islanded microgrids," *Journal of Power Electronics*, Vol. 16, No. 3, pp. 1152-1162, May 2016.

[7] H. Han, X. Hou, J. Yang, and J. Wu, "Review of power sharing control strategies for islanding operation of AC microgrids," *IEEE Trans. Smart Grid*, Vol. 7, No. 1, pp. 200-215, Jan. 2016.

[8] J. M. Guerrero, J. Matas, L. D. Vicuña, M. Castilla, and J. Miret, "Decentralized control for parallel operation of distributed generation inverters using resistive output impedance," *IEEE Trans. Ind. Electron*., Vol. 54, No. 2, pp. 994-1004, Apr. 2007.

[9] J. C. Vasquez, J. M. Guerrero, M. Savaghebi, J. Eloy-Garcia, and R. Teodorescu, "Modeling, analysis, and design of stationary reference frame droop controlled parallel three-phase voltage source inverters," *IEEE Trans. Ind. Electron.*, Vol. 60, No. 4, pp. 1271-1280, Apr. 2013.

[10] J. M. Guerrero, P. C. Loh, T. L. Lee, M. Chandorkar, "Advanced control architectures for intelligent microgrids – Part I: Decentralized and hierarchical control," *IEEE Trans. Ind. Electron.*, Vol. 60, No. 4, pp. 1254-1262, Apr. 2013.

[11] D. E. Olivares, D. E. Olivares, A. Mehrizi-Sani, A. H. Etemadi, C. Canizares, and R. Iravani, "Trends in

microgrid control," *IEEE Trans. Smart Grid*, Vol. 5, No. 4, pp. 1905-1919, Jul. 2014.
[12] S. D'Arco and J. A. Suulet, "Equivalence of virtual synchronous machines and frequency-droops for converter-based microgrids," *IEEE Trans. Smart Grid*, Vol. 5, No. 1, pp. 394-395, Jan. 2014.
[13] Q. C. Zhong and G. Weiss, "Synchronverters: Inverters that mimic synchronous generators," *IEEE Trans. Ind. Electron*., Vol. 58, No. 4, pp. 1259-1267, Apr. 2011.
[14] J. W. He and Y. W. Li, "Analysis, design and implementation of virtual impedance for power electronics interfaced distributed generation," *IEEE Trans. Ind. Appl.*, Vol. 47, No. 6, pp. 2525-2538, Nov./Dec. 2011.
[15] T. L. Vandoorn, J. D. M. D. Kooning, B. Meersman, and L. Vandevelde, "Review of primary control strategies for islanded microgrids with power-electronic interfaces," *Renew. Sustain. Energy Rev.*, Vol. 19, pp. 613–628, Mar. 2013.
[16] T. L. Vandoorn, J. D. M. D. Kooning, B. Meersman, and J. M. Guerrero, "Automatic power sharing modification of P/V droop controllers in low-voltage resistive microgrids," *IEEE Trans. Power Del.*, Vol. 27, No. 4, pp. 2318-2325, Oct. 2012.
[17] J. W. He, Y. W. Li, J. M. Guerrero, J. C. Vasquez, and F. Blaabjerg, "An islanding reactive power sharing scheme enhanced by programmed virtual impedance," in *Proc. of the ISPEDGS*, pp. 229-235, 2012.
[18] X. Yue, Z. Fang, F. Wang, Z. Zhang, and H. Shi, "A novel adaptive frequency injection method for power electronic system impedance measurement," *IEEE Trans. Power Electron.*, Vol. 29, No. 12, pp. 6700-6711, Dec. 2014.
[19] G. Q. Ding, F. Gao, Q. Hao, and S. Zhang, "An improved power sharing control scheme of distributed generation converters in microgrid," in *Proc. of IEEE PEAC*, pp. 372-377, 2014.
[20] Q. C. Zhong, "Robust droop controller for accurate proportional load sharing among inverters operated in parallel," *IEEE Trans. Ind. Electron.*, Vol. 60, No. 4, pp. 1281-1290, Apr. 2013.
[21] J. M. Guerrero, J. C. Vasquez, J. Matas, L. G. D. Vicuña, and M. Castilla, "Hierarchical control of droop-controlled ac and dc microgrids-a general approach toward standardization," *IEEE Trans. Ind. Electron*., Vol. 58, No.1, pp. 158-172, Jan. 2011.
[22] J. W. Simpson-Porco, Q. Shafiee, F. Dorfler, and J. C. Vasquez, "Secondary frequency and voltage control of islanded microgrids via distributed averaging," *IEEE Trans. Ind. Electron*., Vol. 62, No. 11, pp. 7025-7038, Nov. 2015.
[23] Q. Guo, H. Wu, L. Lin, Z. Bai, and H. Ma, "Secondary voltage control for reactive power sharing in an islanded microgrid," *Journal of Power Electronics*, Vol. 16, No. 1, pp. 329-339, Jun. 2016.
[24] E. A. A. Coelho, D. Wu, J. M. Guerrero, and J. C. Vasquez, "Small-signal analysis of the microgrid secondary control considering a communication time delay," *IEEE Trans. Ind. Electron*., Vol. 63, No. 10, pp. 6257-6269, Oct. 2016.
[25] G. Q. Ding, F. Gao, S. Zhang, P. C. Loh, and F. Blaabjerg, "Control of hybrid AC/DC microgrid under islanding operational conditions," *Journal of Modern Power Systems and Clean Energy*, Vol. 2, No. 3, pp. 191-200, Aug. 2014.
[26] C. T. Lee, C. C. Chu, P. T. Cheng, "A new droop control method for the autonomous operation of distributed energy resource interface converters," *IEEE Trans. Power Electron.*, Vol. 28, No. 4, pp. 1980-1993, Apr. 2013.

Guangqian Ding received his B.S. degree in Electronic Information Engineering from the Shandong University of Science and Technology, Qingdao, China, in 2004; and his M.S. and Ph.D. degrees in Electrical Engineering from Shandong University, Jinan, China, in 2010 and 2016, respectively. From 2004 to 2005, he was an Assistant Engineer with LG Innotek Co., Ltd., Huizhou, China. From 2005 to 2012, he was a Project Manager with the State Grid of China Technology College (Shandong Electric Power School), Jinan, China. Since 2016, he has been with the School of Electrical Engineering, University of Jinan, where he is presently working as a Lecturer. His current research interests include power electronics in distributed power systems, microgrids, and power quality.

Feng Gao received his B.S. and M.S. degrees in Electrical Engineering from Shandong University, Jinan, China, in 2002 and 2005, respectively; and his Ph.D. degree from the School of Electrical and Electronic Engineering, Nanyang Technological University, Singapore, in 2009. From 2008 to 2009, he was a Research Fellow at Nanyang Technological University. Since 2010, he has been with the School of Electrical Engineering, Shandong University, where he is presently working as a Professor and serving as a Vice Dean. From September 2006 to February 2007, he was a Visiting Scholar at the Institute of Energy Technology, Aalborg University, Aalborg, Denmark. Dr. Gao received an IEEE Industry Applications Society Industrial Power Converter Committee Prize for a paper published in 2006, and he is presently an Associate Editor of the IEEE TRANSACTIONS ON POWER ELECTRONICS.

Ruisheng Li received his M.S. degree in Power Systems from Xi'an Jiaotong University, Xi'an, China, in 1984. He is presently working as the Deputy Chief Engineer of XJ Electric Co. Ltd., China, and the Deputy Director of its Smart Grid Research Center. He has worked in power system for 25 years and has won numerous awards including a Grand Prize of National Scientific and Technological Progress in 2012. He holds 8 patents and has published more than 30 papers. He was responsible for more than 20 national, provincial and ministerial projects. In addition, he drafted three national standards and three industry standards.

Bingxin Wu received her M.S. degree in Control Theory and Control Engineering from Zhongyuan University of Technology, Zhengzhou, China, in 2009. She is an Engineer in the corporate R&D center of the XJ group. Her current research interests include smart grids, distributed generation, microgrid technology, ac/dc hybrid power grid planning and reliability.